Tailoring solid‐state synthesis routes for high confidence production of phase pure, low impedance Al‐LLZO

Stephen Heywood, Matt Lessmeier, David Driscoll, Stephen Sofie

Tailoring Solid-State Synthesis Routes for High Confidence Production of Phase Pure, Low Impedance Al-LLZO.

Stephen Heywood; Matt Lessmeier; David Driscoll; Stephen Sofie

Department of Mechanical and Industrial Engineering, Montana State University, Bozeman, MT 59717

stephen.heywood@montana.edu
(406) 994-2206

Abstract

Lithium lanthanum zirconium oxide garnet (LLZO) is a solid-state lithium ion conducting electrolyte promising all-solid-state batteries (ASSB) with high charge rates and good energy density due to its chemical stability against lithium metal anodes. LLZO has a high room temperature Li ion conductivity of ~0.1-1 mS/cm in its cubic phase, but the stability of the cubic phase and ionic conductivity are highly sensitive to lithium stoichiometry. Stabilizing agents such as aluminum oxide and excess lithium are needed to preserve the cubic phase and compensate for lithium volatility. With the range of the end LLZO products spanning powders, porous membranes to dense membranes combined with sintering/calcination that often exceeds 1000 ◦C, it is challenging to maintain an ideal lithium content given its high volatility from a single base powder. This study was designed to elucidate the sensitivities of aluminum doped LLZO powder synthesis and processing along its path to being utilized in a ceramic-manufacturing optimized ASSB. By utilizing thermogravimetric analysis in conjunction with in-situ XRD analysis of solid state LLZO synthesis, it was discovered that the sensitivity of the LLZO cubic phase to lithium volatility can be reduced via early incorporation of excess lithium carbonate during initial phase formation in direct combination with controlled surface to volume ratios of the powders. Isostatically pressed powders of our LLZO sintered at 1100 ◦C for 2 hours showed R.T. ionic conductivity of 0.3-0.4 mS/cm measured via EIS, and an improvement in microstructural uniformity with lowered porosity. The improved suppression of lithium volatilization has important implications for the scalable production of LLZO powders and assembly of ASSBs.

1. Introduction

Continuous development since the earliest galvanic cells has enabled energy storage options with ever greater application variety, overall capacity, and reliability. Solid state batteries represent a next frontier with imminent viability[1]. All-solid-state-batteries (ASSBs) promise the likelihood of achieving enhanced safety, charge rate capability, and possibly costs; this is especially true when considering the integrated pack, rather than cell level[2]. A principal driver of interest in ASSBs is the use of lithium metal anodes. Dramatic volumetric energy density and moderate mass specific energy improvements may also be possible due to elimination of cooling systems and the use of higher capacity anodes such as lithium metal[2]. High cell voltage relative to other elements and greatest energy per unit mass makes lithium metal an attractive option[3]. The paradigm of non-aqueous solvent based transport of cations under ambient conditions has provided constraint requiring the use of lithium ion intercalation materials at lower voltages and densities[4]. Leveraging ASSBs to change this paradigm requires effective separator materials.

A wide spectrum of materials has been considered, including perovskites, LiPON, NASICONs, garnets, and sulfides[5]. While sulfides, of several forms, appear to be favored in advanced development for commercialization due largely to manufacturability, they are not without challenge including electrochemical stability[6]. Oxides, especially the $Li_7La_3Zr_2O_{12}$ (LLZO) garnet, have shown electrochemical stability against lithium metal as well as common and high voltage cathode materials, supporting the promise of safe, high-capacity lithium batteries. Over the past decade many doping approaches have succeeded in stabilizing LLZO, but the most stable to the lithium metal system has been with alumina (Al_2O_3) as a substitution into the lattice at a concentration of $Li_{6.25}Al_{0.25}La_3Zr_2O_{12}$[7]. LLZO is primarily impeded as a separator material due to processing challenges associated with high interface resistance, poor mechanical properties, instability in ambient atmosphere, lithium dendrite percolation at the grain boundaries, and lithium volatility during sintering[7,8]. The reward for solving these challenges is a separator material which offers the benefits above, while also allowing operation in extreme environmental conditions such as very high temperature in-situ operation. The ionic conductivity sensitivity to lithium volatilization during sintering is the focus of this work.

For lithium conductivity to reach its peak, LLZO must both remain in its cubic phase and retain an optimum lithium concentration – despite high temperature processing undermining these objectives via lithium volatility[9-15]. This high temperature processing is driven by the distinct requirements of phase formation, and then sintering for densification of a solid separator. Generally speaking, the requirements of sintering a ceramic powder to high enough relative density for bulk ionic conduction are achieving ample particle-particle contact, then dwelling at a temperature exceeding 2/3 material's melting temperature. These requirements present two major issues for LLZO: firstly, the material has 4 separate cations that each have a distinct coordination number with each other all within the same unit cell, complicating the phase formation process and encouraging secondary phases[9-16]. Phases such as lithium zirconate, and aluminates are known to form from mixing heterogeneities prior to thermal consolidation of LLZO precursors[12,16]. Secondly, lithium existing as oxides and carbonates is highly volatile at relevant temperatures[17]. Loss of lithium contributes toward both lower lithium stoichiometry in the cubic phase and generates the insulating impurity lanthanum zirconate ($La_2Zr_2O_7$) pyrochlore[18].

The most common approach to combat lithium loss is to simply dope the precursor powders with excess lithium[17,19]. However, this approach has several limitations in precision regarding the final end product of dense microstructure. Over doping can lead to tetragonal phase formation instead of the desired cubic phase, and moreover is less ideal for ionic conduction[20]. Under doping yields the pyrochlore $La_2Zr_2O_7$ and corresponding loss of cubic phase[18]. The excess lithium added most often as a carbonate vaporizes rapidly, leaving this narrow window of proper excess Li quantity extremely sensitive to powder size and morphology, batch size, calcination profiles and sintering conditions[17, 21]. Variations in both the final microstructure lithium concentration and phase impurity content has generated a wide window of conductivity values ranging on an order of magnitude 10^{-3}- 10^{-4} S/cm within the literature with varied arguments for appropriate levels of excess Li. *This is largely due to an emphasis on studying the phase formation of LLZO from precursors, with lack of emphasis on LLZO in fully densified components; reasonable given that not all architectures propose bulk LLZO components*[19-21].

Additionally, the influence of lithium precursor salt, i.e. lithium hydroxide, nitrate, or carbonate and its effect on final phase formation has been ambiguous. This study explores considerations of lithium precursor effects with the goal of incorporating requisite excess lithium into intermediate and cubic LLZO phases early in calcination such that topical addition of lithium precursor is not subsequently necessary for sintering. The intended effect of this effort is a LLZO powder with functional properties (conductivity) more robust and insensitive to processing conditions. To investigate this relationship, the ionic conductivity of both synthesized and commercially available materials was measured for groups of samples sintered for two different times. The goal of this investigation is to evaluate the influence of deviations in sintering conditions and related lithium concentration on performance of the solid electrolyte, as scale up will introduce analogous deviations as a natural result of larger batches and higher throughput.

More broadly, the ability to mass manufacture LLZO for incorporation into lithium battery designs as a dense ceramic will be contingent on its compatibility with existing ceramic processing techniques including tape casting[17]. An in-situ view of phase formation and lithium volatilization may prove valuable to those hoping to optimize a burnout of green tapes to identify deleterious temperature regimes where LLZO is not yet phase forming but lithium loss is occurring rapidly. The nature of excess lithium doping during initial LLZO synthesis is therefore examined in this study from the perspective of increasing the powder's resilience to lithium loss and secondary phase formation, but also reducing overall ceramic thermal treatment time.

2. Experimental

2.1 Powder Synthesis

Powders for all experimental sets were synthesized using a solid-state route. Numerous processing variations are encompassed in this study, but the standard route from which iterations were varied begins with La_2O_3 (Inframat 57R-0801, batch IMCMH183LAO), ZrO_2 (Inframat 40N-0801, batch IAM10064NZO), Li_2CO_3 (Sigma Aldrich 255823, batch MKCJ1285) and Al_2O_3 (Almatis 16-SG, batch 2025854313) at a stoichiometry of $Li_{6.5}Al_{0.25}La_3Zr_2$, with an excess of 10, 15, and 20 mol% Li^+ with

respect to $Li_{6.5}$ being mixed in an aqueous dispersion and ball milled for 24 hours. The suspension was flash frozen and dried in a Virtis Advantage freeze dryer, where the freeze drying process eliminates settling and heterogeneity. Dry powders were pressed into 1.5 g pellets of 1.905 cm diameter at 250 MPa for calcination. Oxide precursor pellets were calcined for 6 hours at 1100 °C in air supported above the alumina crucible surface by alumina spacer plates at the pellet edges to minimize additional alumina doping. Calcined pellets were ground by mortar and pestle, automatic mortar and pestle, or ball milling. After processing by casting or pressing into new pellets, calcined LLZO was sintered to its final state in an MTI GSL 1500X tube furnace in an argon atmosphere at 1100 °C for 6 hours.

2.2 X-Ray Diffraction

X-ray diffraction was preformed using a Bruker D8 Advance with Cu k-alpha (1.5406 Å). Scans in ambient temperature and atmosphere conditions used stage spinning at 15 revolutions per minute, air scatter knife, and LynxEye detector in 1D, high resolution, mode with a dwell time 0.2 seconds per step. Step sizes varied between 0.01 and 0.08 2θ depending on scan range and resolution required.

In-situ high temperature XRD scans were done using an HTK-1200 temperature stage from RT - 1100 °C with a Kapton/graphite window. Dwell times were increased to 0.5 seconds per step for these measurements. Samples were prepared as loose powders held in aluminum oxide reflection cups.

2.3 Thermal Gravimetric Analysis

Thermal gravimetric analysis (TGA) measurements were made using a Linseis L81 TGA-DTA, where measurements were made in static air with single step ramps from 50 °C – 1100 °C at 5 °C/min. Samples were prepared as mixtures of as-received precursor powder loaded into alumina cups at loadings averaging 130 mg. Instrument sensitivity was set to +-250 mg full scale range.

2.4 Electrochemical Impedance Spectroscopy(EIS)

All pellets were pressed to 1.27 cm diameter at 250 MPa with 200 mg of powder and then sintered with ramp rates of 4 °C/min and dwelled at 1100 °C under Ar flow for 2 hours or 4 hours. Relative density of the sintered pellets was measured via dividing the measured mass by the geometrical volume measured with a micrometer, then actual density divided by theoretical density (5.09g/cm^3). Sintered pellets were 9.5 mm-11 mm in diameter depending on relative density and polished to 300-400 µm thickness. Two sets of sample pellets were introduced, first commercial brand (Ampcera $Li_{6.25}Al_{0.25}La_3Zr_2O_{12}$, Batch: 02120A1) powder pressed and pre-sintered as 1.905 cm pellets at 1100 °C for 2 hours with no added lithium precursor, then ball milled with 20 mol% excess lithium as lithium carbonate relative to $Li_{6.25}$ established by product specifications. The pre-sintering treatment was needed to remove the excess lithium carbonate already present with the product powder, so as to be more comparable to the second sample set: the 20 mol% excess lithium MSU enhanced synthesis and processing calcined samples. Both samples were ball milled for 24 hours in pure ethanol and 2 wt% KD-1 (Tape Casting Warehouse, Lot#2698836) dispersant and dried under ambient atmosphere. See Supplemental Figure S2 for XRD of ball milled powders prior to sintering to confirm presence of cubic LLZO in both.

The pellets were polished with 240 grit SiC paper in the ambient atmosphere for 9 minutes on each side prior to being sputter coated. The pellets were polished adjacent to the sputter coater to minimize transit (air exposure) time, and the first side was re-polished for 30 seconds to minimize extent of impurity formation from reactions with water and carbon dioxide in the air. Pellet edges were masked with carbon tape for the sputtering process. Sputtering was done with gold at 25 mA for 2 minutes per side. One sample was prepared at a time so as to minimize atmospheric exposure, and samples were tested immediately after preparation. EIS was carried out on a Gamry Instruments 1010E Potentiostat, with a perturbation voltage of 25 mV and at frequencies ranging from 1 Hz to 2.5 MHz. The Au/LLZO/Au cell was directly connected to an Arbin-manufactured cell holder interfaced with the potentiostat/EIS. Bulk ionic conductivity was inferred from the diameter of the high frequency arc, which is equivalent to the parallel resistor in the Simplified Randles model[22].

2.5 Preparation for Scanning Electron Microscopy

A Zeiss Supra 55VP field emission scanning electron microscope was used to analyze the sintered EIS pellets with an accelerating voltage of 10 kV. Pellets post-EIS measurements were broken in two halves then sputter coated with iridium with a current of 20 mA for 60 seconds.

Results and Discussion

3.1 Phase Evolution during Oxide-Based Solid State Synthesis

In-situ high temperature XRD (HTXRD) experiments were used to understand principal phase evolutions during solid state synthesis as a function of excess lithium content. Trials across the range of doping levels followed similar overall trends captured in the temperature resolved diffraction patterns shown in Figure 1 below. Intensity is shown as a heat map corresponding to the black being zero intensity and progressively lighter color pointing to higher relative signal intensity. Figure S1 shows the individual diffractograms at each temperature. The data in the figure was derived from a ball milled and freeze-dried mix of oxides loosely calcined in the alumina reflection cup of the XRD stage, which represents a contrast from the refined synthesis protocol of calcining powders as pressed pellets supported over the crucible surface. Discrepancies in the degree of interparticle contact, surface available for Li volatilization, and alumina crucible reaction between HTXRD and the ultimate synthesis protocol are provided as an indicator to elucidate key trends, but not provide a high fidelity representation of phase evolution during the synthesis, which is described later.

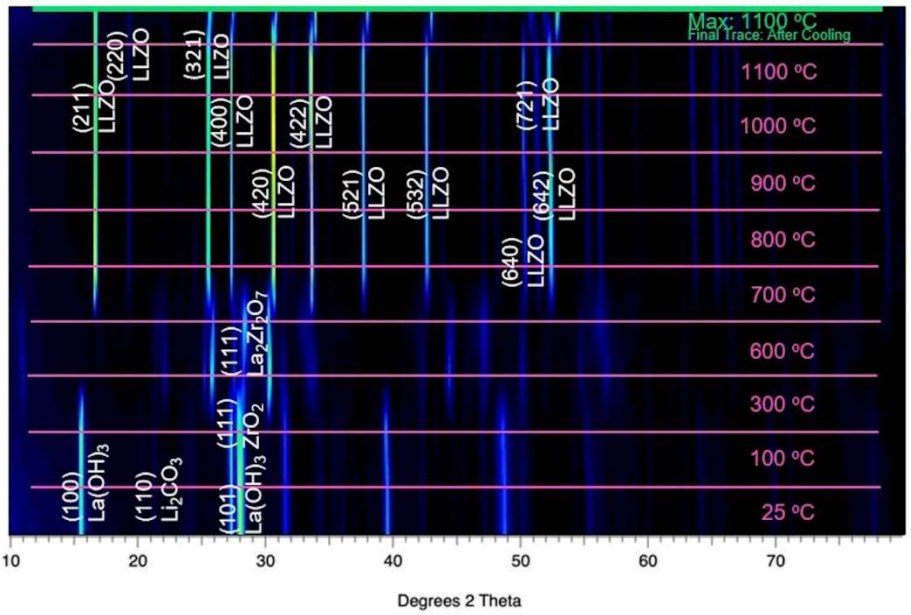

Figure 1: XRD measurement of typical phase evolution of LLZO precursors from room temperature to 1100 °C. This sample was prepared with 15% excess lithium as lithium carbonate. Heatmap indicates dominance of intermediate phases from 300 °C to 800 °C, with garnet dominating at temperatures above 800 °C.

Notable trends in the phase evolution include the oxide precursors with lithium carbonate persisting in near-original form from room temperature to 300 °C after which a number of intermediate phases are observed between 600 °C and 700 °C. A sharp transition is observed from 700 °C where no LLZO is detected to 800 °C where LLZO is dominant evidenced clearly by the (002) peak at 17 °2θ. This trend of precursors persisting to ~400 °C followed by an entirely intermediate composition, with near-full transition to LLZO within a 100 °C window near 800 °C was consistent for all levels of excess Li considered. Ramp rates of the furnace and scan intervals indicate that the degree of conversion shown between 700 °C and 800 °C occurred in less than 20 minutes of elapsed time.

While the compositional transition from intermediate phases to LLZO was observed to be sudden, Figure 1 does indicate that important evolution continues to occur beyond 800 °C. Even if LLZO is immediately dominant, intermediate phases are present through the end of data collection at 1100 °C for the 15 mol% excess Li content shown here. At the same time, as calcination progresses beyond the initial LLZO formation, new impurity phases are observed to grow, observed most readily in multiple peaks from 19-25 °2θ. In

the context of wide variation in sintering/calcination times and temperatures reported in the literature, it is suggested based on this phase evolution that neither the objective of extremely fast calcinations to limit secondary product formation nor especially long times at temperatures to acknowledge slow formation kinetics for LLZO are adequate for the formation of phase-pure garnet and that a more-nuanced approach is required.

It is very well established that the prime contribution to impurity phases after extended calcinations times in LLZO is the difficulty of Li volatilization. This is typically mitigated by the addition of excess Li in the precursor mix to compensate for that lost by evaporation[16-21,23]. Excess Li levels during LLZO syntheses are reported between 10 and 50 mol%[24]. While multiple excess Li levels considered in this study all followed the trends described in Figure 1, the importance of small shifts in excess Li content can be examined in Figure 2 where 5-10 mol% shifts change the onset $La_2Zr_2O_7$ detection by hundreds of degrees during calcination.

The feature of interest in each panel of Figure 2 is the $La_2Zr_2O_7$ (010) reflection at ~28.3 °2θ. $La_2Zr_2O_7$ represents the expected impurity formation as Li loss stoichiometrically limits LLZO formation at these temperatures. For all phases, the peak shifting observed represents the combined effects of thermal expansion in the crystals measured, thermal expansion of the heated stage (z-displacement error), and possible chemically induced lattice strains. For this potentially complex behavior no inferences are made with respect to shifting of peak positions, but instead, relative intensities and onset temperatures for initial phase detection are used to evaluate the effects of excess lithium doping. In the case of 10% excess Li sample, lanthanum zirconate is detected at 900 °C which is delayed until 1000 °C for 15% Li content and is not detected after 1 hour at 1100 °C for 20 % excess Li content studied. The observation that a range of 10 mol% excess Li changes the onset of lanthanum zirconate formation by >200 °C (~65 minutes) during calcination carries a couple of key implications for LLZO synthesis.

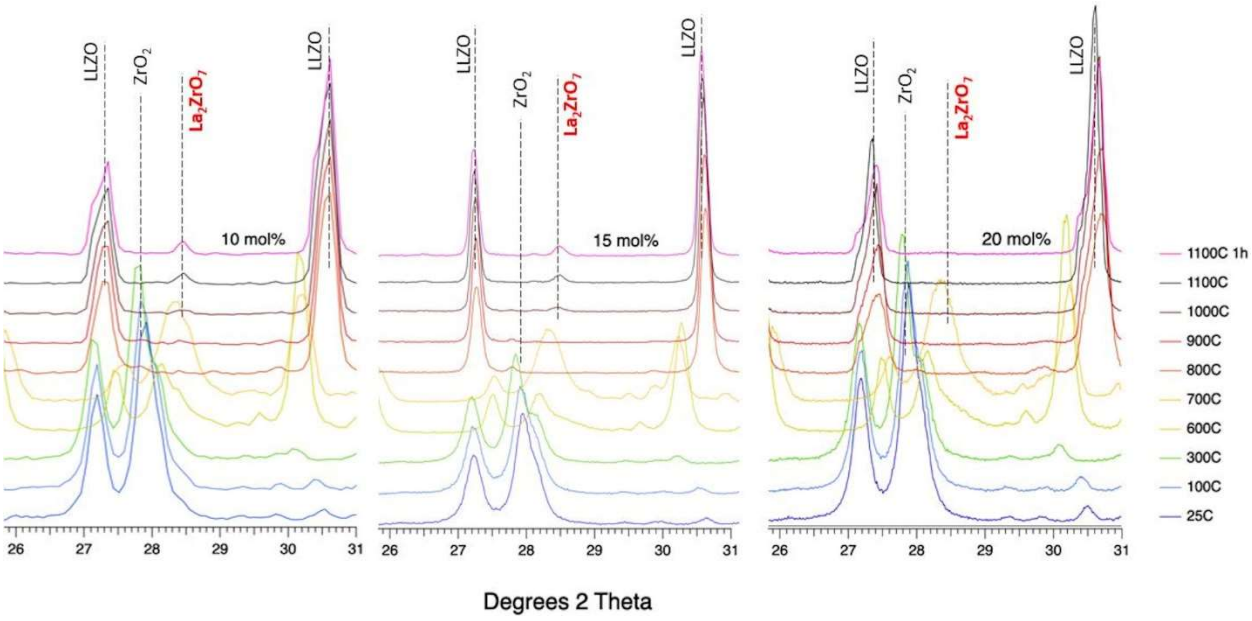

Figure 2: Temperature-resolved XRD measurement of LLZO phase evolution according to excess lithium content. Initial detection of lanthanum zirconate is delayed as excess lithium content increases, to the point of no detection at 20 mol% excess.

First, and consistent with other reports[18,19], the LLZO garnet is not tolerant of Li deficiency. This suggests that in designing an LLZO synthesis, the excess Li content cannot be considered arbitrary or insensitive. Second, the rapid rate of Li loss means that the LLZO formation is very sensitive to processing variations in calcination. In experiments described here, a range of 10 mol% excess Li delayed onset of deleterious phases by >200 ◦C. While solution based synthesis techniques are often considered superior given the inherent homogeneity of solution, the higher surface area particles which tend to result, combined with observations made here may explain the challenges and potential for poorer performance when applying solution based techniques to LLZO synthesis. Though the coarser powders applicable to solid state synthesis are meritorious, Figure 2 suggests that further mitigation of time-temperature sensitivities should be prioritized.

In the scope of possible synthesis pathways considered in this study, less commonly reported alternatives to lithium carbonate as a lithium precursor were considered. Precursor mixtures for LLZO were prepared as

described for the temperature resolved XRD except that lithium carbonate was replaced by lithium hydroxide or lithium nitrate. Lithium nitrate was particularly interesting because of its high water solubility which is expected to have yielded excellent mixing during aqueous ball milling of the precursors. Lithium hydroxide was selected for its low price and accepted industrial use. These powder mixtures were all prepared at an excess Li content of 15 mol% and calcined in a TGA/DTA to 1100 °C and held for 6 hours.

The TGA/DTA curves are shown in Figure 3 where the three alternative precursors are overlaid. All three precursor mixtures show a multistep decomposition beginning with dehydration. Inorganic lithium precursor decomposition is understood to be the final and largest decomposition for all three mixtures. For the hydroxide and nitrate Li precursors, the final decomposition occurs in two stages, initially very rapidly, and then slowing before the resulting oxide mixture slowly evolves Li from the lattice for the remainder of the run. Critically, both the nitrate and hydroxide precursors are observed to begin decomposing just above 400 °C where the carbonate precursor does not begin to decompose until more near 650 °C. These decompositions lead the initial formation of LLZO in Figure 1 by 400 °C and only 150 °C respectively. In the case of the hydroxide precursor mixture, no LLZO was detected. In the case of the nitrate precursor, trace LLZO was detected among numerous phases.

Also significant is the sharp decrease in mass loss rate around 250 minutes for the carbonate and hydroxide precursors and 210 minutes for the nitrate. Based on correlated XRD, it is known that the lithium was not depleted in the case of the carbonate mixture suggesting the interpretation that the rate of Li loss is much lower for Li contained in the LLZO lattice than free lithium carbonate. From the perspective of designing a synthesis which reduces the time-temperature sensitivity of formation, this interpretation reinforces the importance of minimizing the temperature delta between Li precursor decomposition and LLZO formation, which in turn mechanistically supports the use of lithium carbonate.

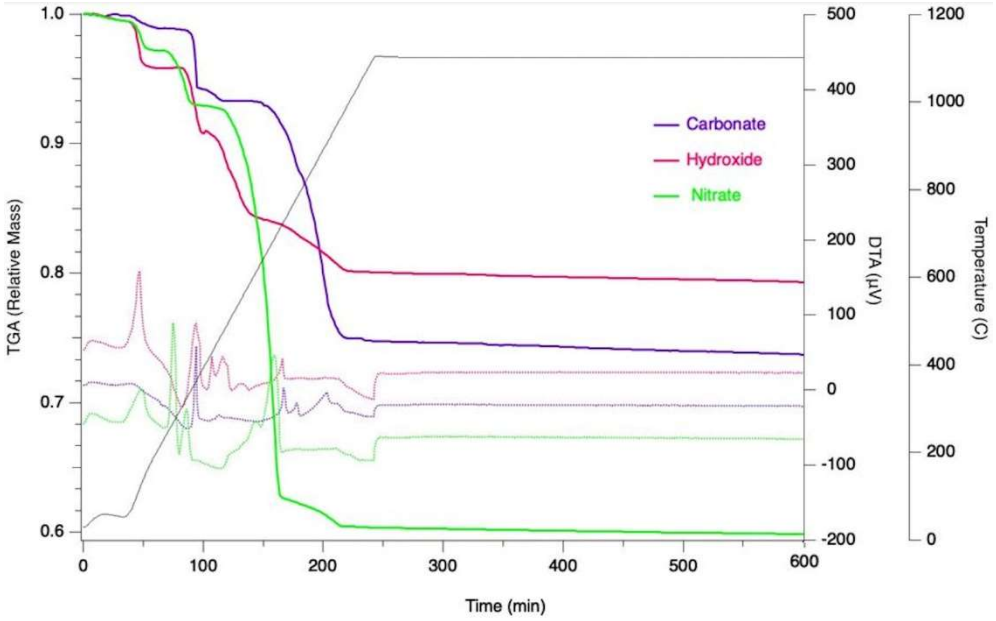

Figure 3: Thermal gravimetric analysis coupled with differential thermal analysis for LLZO precursor mixtures composed of three different lithium sources: carbonate, hydroxide, and nitrate. Note that first mass step of approximately 6% is delayed to highest temperature for carbonate precursor. All precursors indicate a high rate of mass loss until a sudden arrest at approximately 220 minutes/850 ◦C.

3.2 Mitigating Lithium Volatility and Demonstrating Predictability

In sum, the data taken from HTXRD and TGA suggests that solid state synthesis of LLZO from lithium carbonate precursors should be effective. However, it is also suggested that the volatilization problem is so severe that calcination of loose powders may not provide a calcination window where sufficient time exists to fully form cubic LLZO without excessive depletion of Li. The authors iterated the solid-state synthesis protocol to include pressing precursor mixtures into pellets, reducing surface area, and then supporting them at the edges over the crucible surface to reduce alumina contamination[13]. This processing refinement strategy yielded the outcome shown in Figure 4. The stark contrast between surface area-controlled pellets and loose powders further supports the notion of controlling volatility as the driving consideration of the calcination process. This control, for an otherwise replicate synthesis process reduced impurity phases below XRD detection limits and eliminated detection of tetragonal LLZO. This refinement was applied, and an iterative phase formation study was again conducted varying levels of excess Li to produce Figure 5.

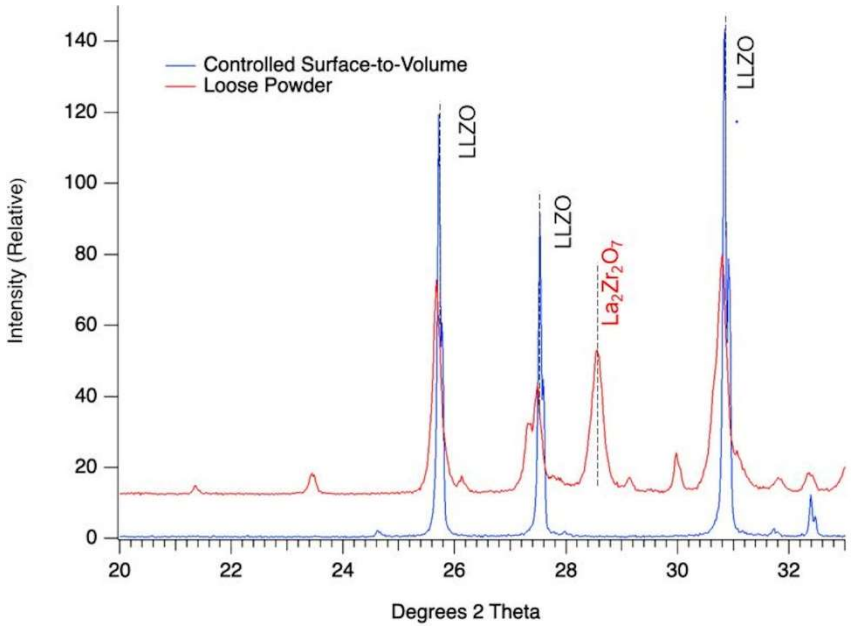

Figure 4: Comparison of controlled surface to volume ratio calcinations with pressed pellets vs loose powder calcinations in identical alumina crucibles. Loose powder shows a marked disadvantage in lithium volatilization displayed by the pronounced growth of lithium deficient pyrochlore phase.

Figure 5 compares the outcomes of calcination of the three precursor mixtures for 6 hours at 1100 °C against commercially available LLZO doped with Al. It is clear from the 28.3 °2θ peak that 10 mol% initial excess is inadequate resulting in lanthanum zirconate formation. No lanthanum zirconate was detected for the 15 mol% doping level and was possibly detected at 20%. This compares favorably with the commercial powder which, in the as-received state, indicated possibly detected lanthanum zirconate. In addition, the commercial powder shows remaining lithium carbonate (possibly added as excess for sintering), and a small peak at 23.6 °2θ which correlates with $LiAlO_2$. The internally produced LLZO's show doped-Al_2O_3 which was not incorporated in the LLZO during calcination. Using the controlled surface-to-volume ratio of pressed pellets for sample sets, the in-house synthesized powder outperforms the commercially available variant. This discrepancy is explored in Figure 8 where the evolution of microstructural density and gas transport pathways is discussed.

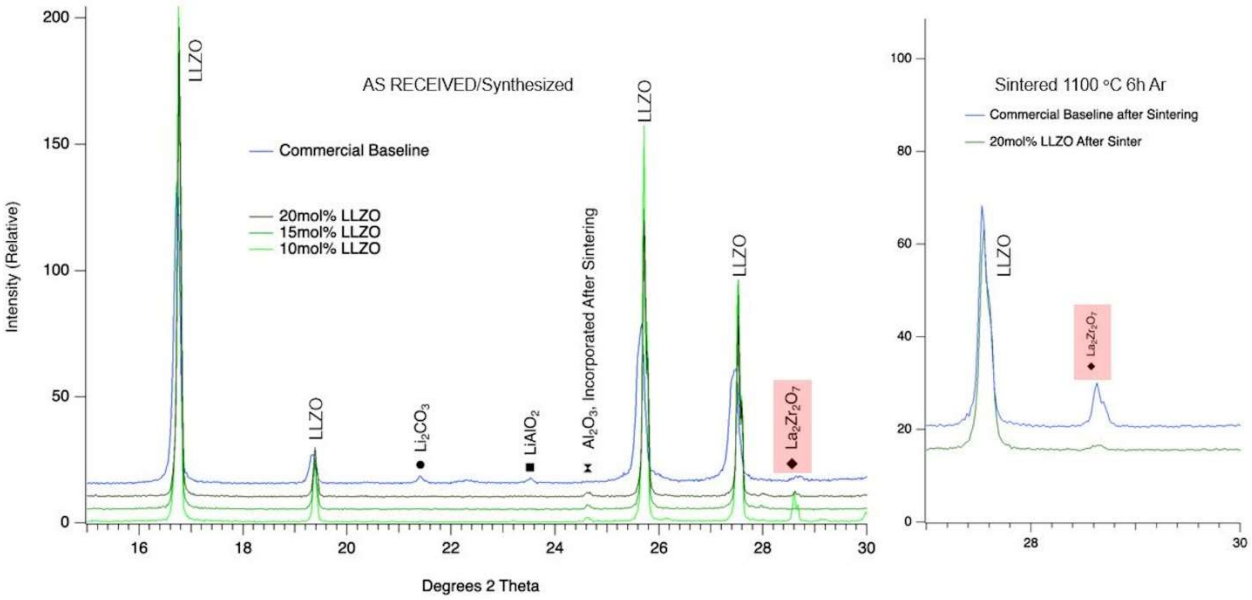

Figure 5: Outcomes of calcination process compared by XRD. Calcination conducted at 1100 °C for 6 hours in an air atmosphere. Three excess lithium content samples compared with as-received powder from commercial vendor.

Of course, calcination achieves the objective of phase formation, but when the material is used in an all-solid-state architecture without polymeric additives, sintering of the LLZO to high density in the appropriate form factor is required. This condition imposes the constraint that the "as-received" or "as-calcined" state of LLZO is of limited relevance to battery performance relative to the "post-sintering/processing state." A processing flow diagram depicting the steps used in this study to synthesize LLZO followed by generic post processing steps are shown in Figure 6. An important metric of powder quality in a functional environment is its sensitivity to the processing steps subsequent to calcination.

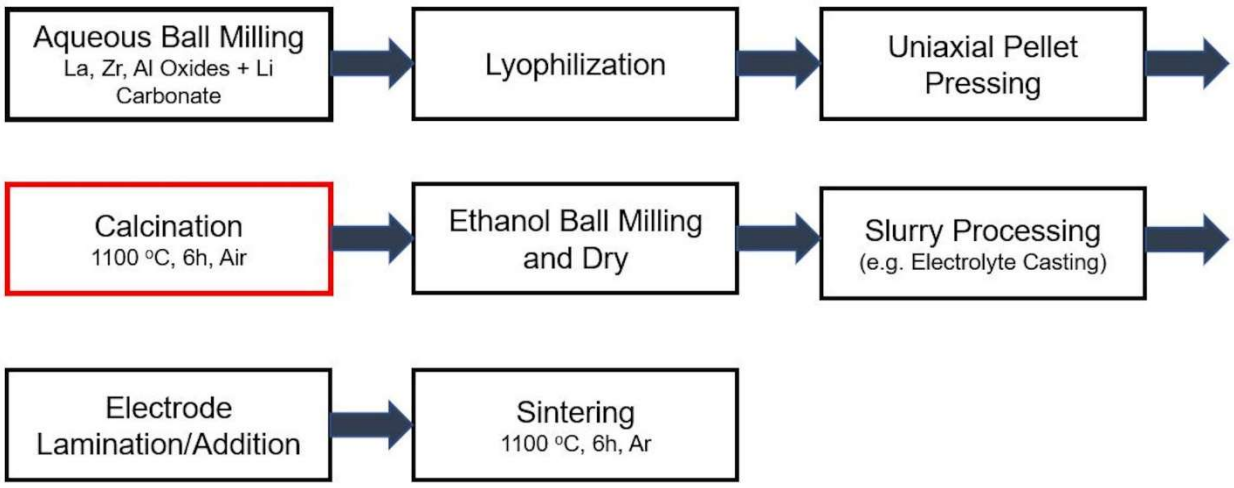

Figure 6: Generalized process flow diagram for LLZO produced by solid state reaction of oxides of La, Zr, and Al with lithium carbonate. Above approach consistently yields phase-pure (within XRD detection limits) cubic LLZO.

LLZO is recognized as being very sensitive to humidity which leads to surface layers of Li_2CO_3[25]. The authors of this study frequently employ water-based slurry processing techniques that vital to scalable battery manufacture. To partially simulate this casting and explore more directly sintering effects, the 15 mol% excess powder of Figure 5 and commercial powder were pressed into pellets using water as a pressing binder and sintered under Ar for 6 hours at 1100 °C. Resulting pellets were ground by mortar and pestle and analyzed by XRD shown in Figure 7.

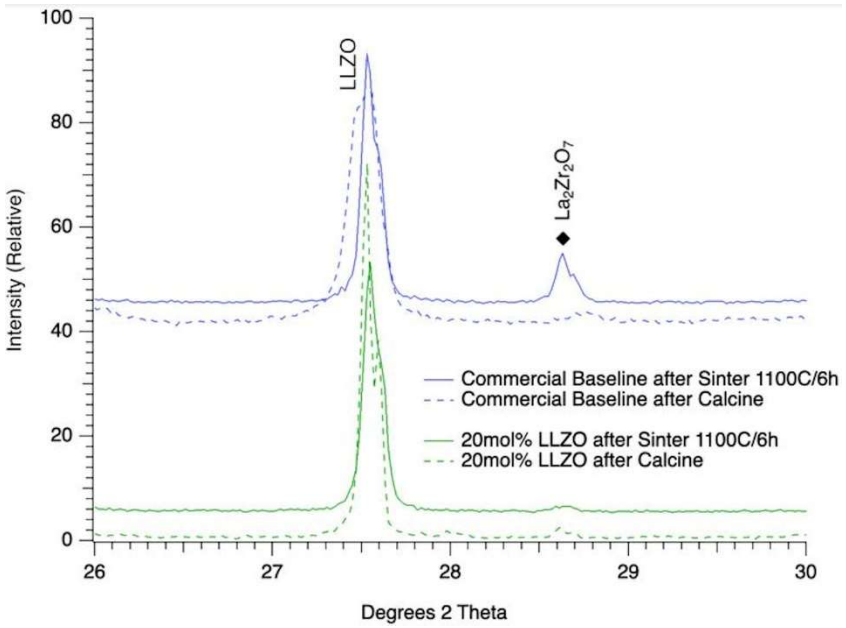

Figure 7: Comparison of MSU and commercial powders after calcination (as received; commercial), and after sintering 1100 °C, 6 hours, in Argon. $La_2Zr_2O_7$ phase formation suppressed in the lattice doped LLZO relative to standalone pre-phase formed LLZO.

For both the internally synthesized powder and commercial baseline, the only detected impurity post sintering was $La_2Zr_2O_7$. No additional Li_2CO_3 was added to either powder prior to sintering. Significantly, the internally synthesized LLZO shows very little evolution above detection limits with good phase purity meeting an important definition of low processing sensitivity. The commercial powder retained a major fraction of cubic LLZO, though an easily detectable quantity of insulating $La_2Zr_2O_7$ was observed.

From the understanding that the commercial baseline powder loses much of its lithium and cubic phase purity, a comparison was made to elucidate whether the quantity of excess lithium present in our 20 mol% excess powder was comparable to the commercial powder control sample. Lower density and more inconsistency/higher impedance was observed from the unmodified commercial baseline powder sintered at 1100 °C for 2 hours measured by EIS, with sample to sample ionic conductivity ranging from 1.1 – 8.6 x 10^{-5} S/cm. Impedance of commercial baseline may be reduced by simply grinding and remixing already sintered pellets with a controlled level of excess lithium carbonate and then pressing and sintering again. That hypothesis became the rationale for milling and adding 20 mol% excess lithium to the

commercial LLZO sample, so that any excess lithium that was present from the factory would not contribute to total effective conductivity while having a similar level of lithium to our in house produced powder. Both the densification and ionic conductivity appeared to have been improved by this approach, but with a caveat that it still has lower conductivity relative to our enhanced synthesis processed powders.

3.3 Electrochemical & Sintering Performance

The Nyquist plots from EIS data can be seen in Figure 8. The in-house synthesized material sintered at 1100 °C for 2 hours had the lowest impedance and highest ionic conductivity. Both the commercial and synthesized materials sintered for 2 hours showed higher ionic conductivity than their 4 hour counterparts, supporting 1100 °C and 2 hours as the optimal sintering parameters for this particular stoichiometry and Li excess. Both in house synthesized sets, the 2 hour and 4 hour sintering hold times, performed better than the excess lithium modified commercial baseline. The merit of excess lithium carbonate incorporation in the precursor powder mixture before calcining became clear from the lowered impedance, as opposed to topical incorporation in already phase formed commercial powder mixture before sintering. The apparent bulk conductivities appear to be valid comparisons with only slight variations in density observed between sample sets. In-house synthesized 2 hour materials were 86-87% dense, synthesized 4 hour materials were 78-82% dense, with commercial 2 hour materials being 81% dense, and commercial 4 hour materials being 77-82% dense. For all samples, the impedance response was typical of that expected for an Au-plated conductor which allowed fitting by the Simplified Randles Model which is discussed elsewhere[26]. This fit was used to derive an estimate of bulk Li^+ conductivities[22]. For the 2 hour sintered materials, the estimated conductivities of the solid-state synthesized pellets were 3.2 – 4.0 x 10^{-4} S/cm and 0.88 – 0.99 x 10^{-4} S/cm for the modified commercial baseline.

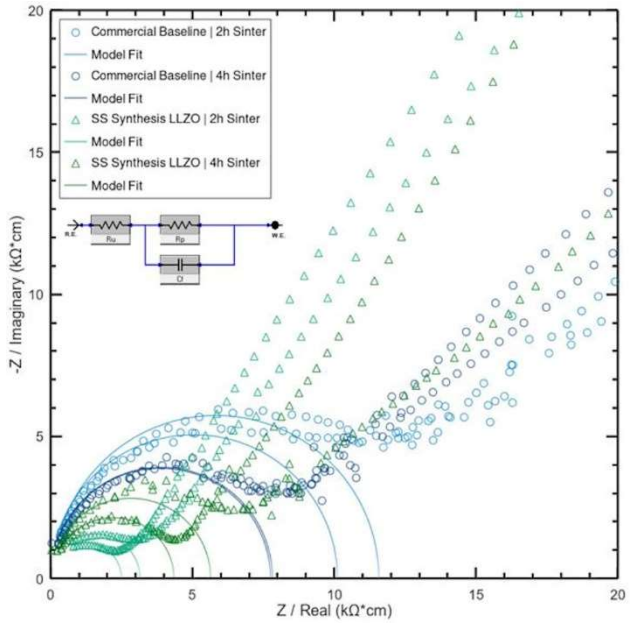

Figure 8: Electrical impedance spectroscopy (EIS) comparison of LLZO pellets with commercial powder sintered with 20% excess Li^+ milled into powder, and MSU production LLZO pellet containing 20 mol% calcined, milled and sintered. Both pellets sintered at 1100 °C at 4 °C/min ramp and 2 hour or 4 hour dwell time. Note that these commercial baseline samples are not 'as-received' from the prior XRD data in Figure 7.

In Figure 9, the topically doped commercial LLZO is compared to the enhanced synthesis and processing doped LLZO in the form of fracture surfaces of the pellets utilized in the EIS data. Figure S3 shows the extra set of sintered LLZO for 4 hours.

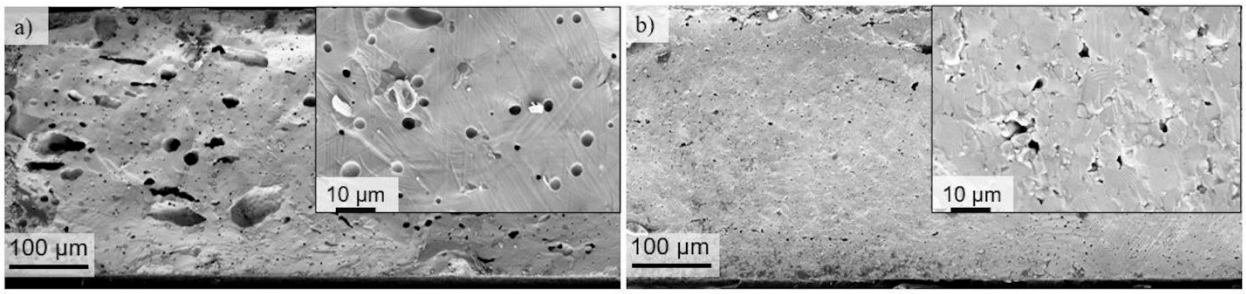

Figure 9: Compared fracture surface microstructures of EIS LLZO pellets with commercial powder a) sintered with 20% excess Li^+ milled into powder, and b) MSU production EIS LLZO pellet containing 20 mol% calcined, milled and sintered. Both pellets sintered at 1100 °C at 4 °C/min ramp and 2 hour dwell time. Macropores present in sample a) demonstrate more rapid evolution of lithium carbonate decomposition products.

A requirement of LLZO used as a solid state separator is lack of open porosity. The reduction of porosity is intrinsically paired to the densification of the microstructure, and it has been demonstrated that greater ionic conductivity comes with extensive sintering of grains[27]. This work underscores a secondary effect of lithium volatility in LLZO causing macropores to open that are 10-80 μm in size. This effect is demonstrated in samples with excess Li_2CO_3 doping during the milling process, which would be a common technique for preparing powders for tape casting. The samples produced with the in-lattice doping & controlled calcination strategy under identical sintering conditions demonstrate a lack of abundant macro-pores within the ½ inch ~300 μm thick sintered pellets. Both structures exhibited transgranular fracture patterns which indicated good densification, the volatilization of lithium did appear to severely affect the overall porosity and the EIS data acquired from each pellet. Although many porous membranes across literature are below 100 μm such that they are thin enough to mitigate trapping of escaping gasses[7], our XRD data in conjunction with the macroporosity observations demonstrate a trend towards less than ideal escape of lithium is what creates these voids. Ordinarily, extended sintering durations[8,19,28-30], hot-pressing, field assisted, or spark-plasma sintering are needed to achieve an elevated level of microstructural uniformity in bulk sintered LLZO pellets. The other common approach of utilizing a mother powder of lithium[24] or saturation of LLZO's atmosphere with Li_2O to suppress its volatilization are viable but may restrict applied scalability if surplus lithium supply becomes too costly[31]. Overall, optimized synthesis and processing parameters that reduce topically added lithium precursor enable the end user to dial in on a lower impedance for membrane production. The coarse addition of excess lithium, while still reasonably effective, lacks the edge of precise lithium additions, calcination, and sintering time parameters.

Conclusions

The solid-state synthesis of aluminum doped LLZO has been thoroughly investigated and further optimized through experimental activities to refine the understanding of the relationship between lithium volatility, phase formation, and ionic conductivity. Both the cubic LLZO synthesis, and post phase formation processing are not only sensitive to lithium volatility, but also to methods for excess lithium insertion which dramatically affect the rate of phase transformations necessary for the formation of cubic garnet structure. Compaction

of powder during phase formation above 1000 °C has a marked improvement in garnet stabilization. The implications are of profound importance for scaling powder production and sintering for all-solid-state batteries at an industrial scale. Not only must surface to volume ratio be considered, and likely controlled to account for lithium loss, but proper incorporation of lithium precursors can reduce volatility and thermal sensitivity to make mass production considerably less tenuous. A uniform microstructure as a product of lithium volatility reduction demonstrates significant benefits to ionic conductivity. Deliberately controlled interplay of each powder processing variable towards a target membrane application is critical to boosting ionic conductivity whether sintering or polymeric compositing is utilized.

Acknowledgements

Research was sponsored by the DEVCOM Army Research Laboratory (ARL) and was funded under Cooperative Agreement (CA) Number W911NF-20-2-0284. The views and conclusions contained in this document are those of the authors and should not be interpreted as representing the official policies, either expressed or implied, of the DEVCOM Army Research Laboratory or the U.S. Government. The U.S. Government is authorized to reproduce and distribute reprints for Government purposes notwithstanding any copyright notation hereon.

Additional acknowledgement goes to the Montana State University Imaging and Chemical Analysis Laboratory for use of temperature resolved XRD and FESEM microscopy equipment.

References

1. Sun C, Liu J, Gong Y, Wilkinson DP, Zhang J. Recent advances in all-solid-state rechargeable lithium batteries. Nano Energy. 2017;33:363–86.

2. Schnell J, Günther T, Knoche T, Vieider C, Köhler L, Just A, et al. All-solid-state lithium-ion and lithium metal batteries – paving the way to large-scale production. J Power Sources. 2018;382:160–75.

3. Lin D, Liu Y, Cui Y. Reviving the lithium metal anode for high-energy batteries. Nat Nanotechnol. 2017;12:194–206.

4. Kiani MA, Mousavi MF, Rahmanifar MS. Challenges in the development of advanced Li-ion batteries: a review. Energy Environ Sci. 2011;4:3243–62.

5. Bachman JC, Muy S, Grimaud A, Chang HH, Pour N, Lux SF, et al. Inorganic Solid-State Electrolytes for Lithium Batteries: Mechanisms and Properties Governing Ion Conduction. Chem Rev. 2016;116:140–62.

6. Gao Z, Sun H, Fu L, Ye F, Zhang Y, Luo W, et al. Promises, Challenges, and Recent Progress of Inorganic Solid-State Electrolytes for All-Solid-State Lithium Batteries. Adv Mater. 2018;30:1–27.

7. Samson AJ, Hofstetter K, Bag S, Thangadurai V. A bird's-eye view of Li-stuffed garnet-type $Li_7La_3Zr_2O_{12}$ ceramic electrolytes for advanced all-solid-state Li batteries. Energy Environ Sci. 2019;12:2957–75.

8. Ramakumar S, Deviannapoorani C, Dhivya L, Shankar LS, Murugan R. Lithium garnets: Synthesis, structure, Li^+ conductivity, Li^+ dynamics and applications. Prog Mater Sci. 2017;88:325–411.

9. Chen Y, Rangasamy E, Cruz CR, Liang C, An K. A study of suppressed formation of low-conductivity phases in doped $Li_7La_3Zr_2O_{12}$ garnets by in situ neutron diffraction. J Mater Chem A. 2015;3:22868–76.

10. Matsuda Y, Sakamoto K, Matsui M, Yamamoto O, Takeda Y, Imanishi N. Phase formation of a garnet-type lithium-ion conductor $Li_{7-3x}Al_xLa_3Zr_2O_{12}$ Solid State Ionics. 2015;277:23–9.

11. Matsui M, Sakamoto K, Takahashi K, Hirano A, Takeda Y, et al. Phase transformation of the garnet structured lithium ion conductor: $Li_7La_3Zr_2O_{12}$. Solid State Ionics. 2014;262:155–9

12. El-Shinawi H, Paterson GW, MacLaren DA, Cussen EJ, Corr SA. Low-temperature densification of Al-doped $Li_7La_3Zr_2O_{12}$: a reliable and controllable synthesis of fast-ion conducting garnets. J Mater Chem A. 2017;5:319–29.

13. Xia W, Xu B, Duan H, Guo Y, Kang H, Li H, et al. Ionic Conductivity and Air Stability of Al-Doped $Li_7La_3Zr_2O_{12}$ Sintered in Alumina and Pt Crucibles. ACS Appl Mater Interfaces. 2016;8:5335–42.

14. Hu Z, Liu H, Ruan H, Hu R, Su Y, Zhang L. High Li-ion conductivity of Al-doped $Li_7La_3Zr_2O_{12}$ synthesized by solid-state reaction. Ceram Int. 2016;42:12156–60.

15. Thompson T, Wolfenstine J, Allen JL, Johannes M, Huq A, David IN, et al. Tetragonal vs. cubic phase stability in Al – free Ta doped $Li_7La_3Zr_2O_{12}$ (LLZO). J Mater Chem A. 2014;2:13431–6.

16. Rosenkiewitz N, Schuhmacher J, Bockmeyer M, Deubener J. Nitrogen-free sol-gel synthesis of Al-substituted cubic garnet $Li_7La_3Zr_2O_{12}$ (LLZO). J Power Sources. 2015;278:104–8.

17. Yi E, Wang W, Kieffer J, Laine RM. Flame made nanoparticles permit processing of dense, flexible, Li^+ conducting ceramic electrolyte thin films of cubic- $Li_7La_3Zr_2O_{12}$ (c-LLZO). J Mater Chem A. 2016;4:12947–54.

18. Quinzeni I, Capsoni D, Berbenni V, Mustarelli P, Sturini M, Bini M. Stability of low-temperature $Li_7La_3Zr_2O_{12}$ cubic phase : The role of temperature and atmosphere. Mater Chem Phys. 2017;185:55–64.

19. Rangasamy E, Wolfenstine J, Sakamoto J. The role of Al and Li concentration on the formation of cubic garnet solid electrolyte of nominal composition $Li_7La_3Zr_2O_{12}$. Solid State Ionics. 2012;206:28–32.

20. Zhang Y, Chen F, Tu R, Shen Q, Zhang X, Zhang L. Effect of lithium ion concentration on the microstructure evolution and its association with the ionic conductivity of cubic garnet-type nominal $Li_7Al_{0.25}La_3Zr_2O_{12}$ solid electrolytes. Solid State Ionics. 2016;284:53–60.

21. Chen R, Huang M, Huang W, Shen Y, Lin Y, Nan C. Effect of calcining and Al doping on structure and conductivity of $Li_7La_3Zr_2O_{12}$ Solid State Ionics. 2014;265:7–12.

22. Wolfenstine J, Rangasamy E, Allen JL, Sakamoto J. High conductivity of dense tetragonal $Li_7La_3Zr_2O_{12}$. J Power Sources. 2012;208:193–6.

23. Xu B, Duan H, Xia W, Guo Y, Kang H, Li H, et al. Multistep sintering to synthesize fast lithium garnets. J Power Sources. 2016;302:291–7.

24. Liu K, Ma J, Wang C. Excess lithium salt functions more than compensating for lithium loss when synthesizing $Li_{6.5}La_3Ta_{0.5}Zr_{1.5}O_{12}$. J Power Sources. 2014;260:109–14.

25. Xia W, Xu B, Duan H, Tang X, Guo Y, Kang H, et al. Reaction mechanisms of lithium garnet pellets in ambient air : The effect of humidity and CO_2. J Am Ceram Soc. 2017;100:2832–9.

26. Sastre J, Futscher MH, Pompizi L, Aribia A, Priebe A, Overbeck J, et al. Blocking lithium dendrite growth in solid-state batteries with an ultrathin amorphous Li-La-Zr-O solid electrolyte. Commun Mater. 2021;2:76.

27. Neumann A, Hamann TR, Danner T, Hein S, Becker-Steinberger K, Wachsman E, et al. Effect of the 3D Structure and Grain Boundaries on Lithium Transport in Garnet Solid Electrolytes. ACS Appl Energy Mater. 2021;4:4786–804.

28. Botros M, Djenadic R, Clemens O, Möller M, Hahn H. Field assisted sintering of fine-grained $Li_{7-3x}La_3Zr_2Al_xO_{12}$ solid electrolyte and the influence of the microstructure on the electrochemical performance. J Power Sources. 2016;309:108–15.

29. Ni JE, Case ED, Sakamoto JS, Rangasamy E, Wolfenstine JB. Room temperature elastic moduli and Vickers hardness of hot-pressed LLZO cubic garnet. J Mater Sci. 2012;47:7978–85.

30. Yamada H, Ito T, Hongahally R, Bekarevich R, Mitsuishi K. Influence of strain on local structure and lithium ionic conduction in garnet-type solid electrolyte. J Power Sources. 2017;368:97–106.

31. Huang X, Lu Y, Song Z, Rui K, Wang Q, Xiu T. Manipulating Li_2O atmosphere for sintering dense $Li_7La_3Zr_2O_{12}$ solid electrolyte. Energy Storage Mater. 2019;22:207–17.